Published in final edited form as:

Neuroimage. 2022 September ; 258: 119339. doi:10.1016/j.neuroimage.2022.119339.

Brain intrinsic connection patterns underlying tool processing in human adults are present in neonates and not in macaques

Haojie Wen[a,b,c], **Ting Xu**[d], **Xiaoying Wang**[a,b,c], **Xi Yu**[a,*], **Yanchao Bi**[a,b,c,e,*]

[a]State Key Laboratory of Cognitive Neuroscience and Learning, Beijing Normal University, Beijing 100875, China

[b]IDG/McGovern Institute for Brain Research, Beijing Normal University, Beijing 100875, China

[c]Beijing Key Laboratory of Brain Imaging and Connectomics, Beijing Normal University, Beijing 100875, China

[d]Center for the Developing Brain, Child Mind Institute, New York, NY 10022, USA

[e]Chinese Institute for Brain Research, Beijing 102206, China

Abstract

Tool understanding and use are supported by a dedicated left-lateralized, intrinsically connected network in the human adult brain. To examine this network's phylogenetic and ontogenetic origins, we compared resting-state functional connectivity (rsFC) among regions subserving tool processing in human adults to rsFC among homologous regions in human neonates and macaque monkeys (adolescent and mature). These homologous regions formed an intrinsic network in human neonates, but not in macaques. Network topological patterns were highly similar between human adults and neonates, and significantly less so between humans and macaques. The premotor-parietal rsFC had most significant contribution to the formation of the neonatal tool network. These results suggest that an intrinsic brain network potentially supporting

*Corresponding authors at: State Key Laboratory of Cognitive Neuroscience and Learning, Beijing Normal University, Beijing 100875, China. xi.yu@bnu.edu.cn (X. Yu), ybi@bnu.edu.cn (Y. Bi).

Data and code availability statement

The human adult and neonate datasets are available at https://www.humanconnectome.org/ and https://www.developingconnectome.org, respectively. The macaque data are available at http://fcon_1000.projects.nitrc.org/indi/indiPRIME.html. For the macaque data, subject IDs included in the current study are listed in Supplementary Table S1, and the computed network results are available at https://github.com/xiyu-bnu/neonate_tool_network. Moreover, the codes for the cross-species alignment are available at https://github.com/TingsterX/alignment_macaque-human. Due to HCP and dHCP privacy policies, the preprocessed resting-state images of human adults and neonates (with their IDs) can only be shared upon request with qualified investigators who agree to the Restricted Data Use Terms of these two datasets.

Declaration of Competing Interest

The authors declare no competing interests.

Credit authorship contribution statement

Haojie Wen: Conceptualization, Methodology, Formal analysis, Investigation, Writing – review & editing, Writing – original draft, Visualization. **Ting Xu:** Methodology, Writing – review & editing. **Xiaoying Wang:** Conceptualization, Methodology, Writing – review & editing, Funding acquisition. **Xi Yu:** Conceptualization, Methodology, Formal analysis, Writing – original draft, Writing – review & editing, Visualization, Supervision, Funding acquisition. **Yanchao Bi:** Conceptualization, Methodology, Writing – original draft, Writing – review & editing, Supervision, Funding acquisition.

Supplementary materials

Supplementary material associated with this article can be found, in the online version, at doi:10.1016/j.neuroimage.2022.119339.

tool processing exists in the human brain prior to individual tool use experiences, and that the premotor-parietal functional connection in particular offers a brain basis for complex tool behaviors specific to humans.

Keywords

Tool brain network; Macaque; Neonate; Resting-state fMRI; Phylogeny; Ontogeny

1. Introduction

Complex and flexible tool making and tool use are argued to be unique to homo sapiens (Ambrose, 2001; Gibson et al., 1994; Oakley, 1956; Vaesen, 2012; Laland and Seed, 2021). Such abilities are aligned with observations of a dedicated left-lateralized network in human adult brain that is particularly relevant for processing tools (e.g., hammers, axes, scissors), which includes left lateral occipital-temporal cortex (LOTC), inferior and superior parietal lobule, inferior frontal gyrus, and premotor cortex. These regions are preferentially activated when human adults view pictures of tools relative to other types of objects (e.g., faces, animals, and large, non-manipulable objects), listen to tool names, imagine tool use, or pantomime tool use (Chao and Martin, 2000; Chouinard and Goodale, 2012; Lewis, 2006; Peelen et al., 2013; Wang et al., 2018; for a review see Bi et al., 2016). Also, they have been observed to be both structurally and functionally connected (Bi et al., 2015; Konkle and Caramazza, 2017; Peelen et al., 2013) and lesions to these regions and/or to their underlying white matter connections can lead to deficits in tool understanding and use (Bi et al., 2015; Buxbaum et al., 2014; Garcea et al., 2020; Tarhan et al., 2015). It is assumed that these regions contribute multiple types of computations to tool processing, with the LOTC, as part of the ventral visual pathway, involved in visual shape analysis and, optimally connected to the parietal and frontal regions to support grasping, manipulating and (conceptual) understanding tools (Mahon, 2020).

What are the phylogenetic and ontogenetic origins of the tool processing network observed in human adults? Is its formation simply the result of associative learning, based on individual experiences of tool manipulation, which bridge sensory and motor representations of tools? Or is this network (partly) innate, predisposed in the human brains prior to any individual object use experience, and potentially human-specific, given its evolutionary significance in homo sapiens? One way to tackle this fundamental question is to compare this brain system in human adults with that in human neonates and non-human animals. However, it is difficult to perform tool-processing experimental tasks with human neonates not only for practical reasons but also because of highly limited cognitive/motor skills (only reflective motor responses, without grasping/manipulating abilities). The approach we took here, motivated by the notion that brain function is determined by connection patterns (Passingham et al., 2002), is to take advantage of resting-state functional connectivity (rsFC) data and examine whether the intrinsic brain connection pattern among the homologous brain regions of interest are already in place in human neonates.

Regarding nonhuman primates, similarities and differences to humans have been reported on both behavioral and neural levels. The simpler forms of tool use and even tool making are not unique to humans. Animals have visual and motor experiences with objects such as gasping a stick, and some have even demonstrated simple tool use (e.g., apes and crows use sticks to forage for insects, Bentley-Condit and Smith, 2010; Fayet et al., 2020; Shumaker et al., 2011). Nevertheless, humans are arguably the only species that can make and use sophisticated tools based on causal (mechanical) understanding of the relationship between its physical properties, use and function (Johnson-Frey, 2003; Laland and Seed, 2021; Osiurak and Reynaud, 2020; Penn et al., 2008; Vaesen, 2012; Visalberghi and Limongelli, 1994), which allows them to convert ordinary objects into tools for flexible functional use as early as two years of age (Kastner et al., 2017). Neurally, in the macaque brains, object grasping or simple-tool-use is supported by a lateral network encompassing the parietal cortex, premotor area and inferior frontal gyrus (e.g., Borra et al. 2017, Obayashi et al. 2001), regions in proximity to the tool-processing areas in human adults; yet, species-differences were observed in the left inferior parietal cortex associating with tool-use-activities (Peeters et al., 2009). The characteristics of brain connectivity pattern among these homologous brain regions, however, have not been compared across species and developmental trajectories.

Here, we empirically tested the phylogenetic and ontogenetic origins of the intrinsic tool processing network observed in human adults by comparing resting-state functional connectivity (rsFC) pattern among tool processing regions in human adults (n = 100) to rsFC among homologous regions in human neonates with little motor experience (n = 118) and in macaque monkeys with ample visual/motor experiences (adolescent and mature, n = 25). If the emergence of the intrinsically connected tool processing network in human adults is driven by learnt sensory-motor association based on the visual-motor/manipulation experiences with objects, then similar intrinsic connectivity pattern among the homologous regions are not predicted in human neonates, who have not developed any nonreflective motor skills and thus no object use experience, but predicted in macaques, who have extensive motor experience with objects. Alternatively, the tool network observed in human adults may be innate and (at least partly) unique to homo sapiens, supporting the human-unique complex tool making/use behaviors, and we would expect to observe similar intrinsic connectivity pattern already present among the homologous regions in the human neonate brain, and not in the macaque brain. A brain network supporting face processing (henceforth face processing network), which has been reported for both humans (Wang et al., 2016) and macaques (Schwiedrzik et al., 2015), was also assessed in these three populations as a reference point for the potential tool processing network.

2. Methods

2.1. Participants

Human adults.—Resting-state images of human adults were obtained from the WU-Minn Human Connectome Project (HCP) carried out at Washington University in St. Louis (Van Essen et al., 2013, https://www.humanconnectome.org/study/hcp-young-adult). For the current study, 100 individuals (55 females, 28.3 ± 3.4 years old), coming from different

families (i.e., not related), were randomly selected from the 1200 Subjects Data Release. The fMRI data of all selected participants met the following inclusion criteria: (1) had less than 10% of volumes with framewise displacement (FD) ≥ 0.3 mm (see details in 2.2 Image preprocessing) and (2) exhibited good coverage (>50% overlap) of the functional Regions of Interest (ROIs) selected (see details in 2.4 ROI selection and cross-population registration). This project was reviewed and approved by the Institutional Ethics Committee of Washington University in St. Louis, Missouri. All participants signed written informed consent.

Human neonates.—Imaging data of human neonates were obtained from the Developing Human Connectome Project (dHCP) conducted at the Newborn Imaging Center at Evelina London Children's Hospital, London, UK (Makropoulos et al., 2018, https://www.developingconnectome.org). 118 neonates (57 females, birth age = 39.7 ± 1.9 weeks; scan age = 40.9 ± 2.1 weeks, birth weight = 3.1 ± 0.66 kg) were selected from the two data releases available at the time of data analysis for the present study based on the following inclusion criteria: (1) images were acquired within the first month (i.e., ≤ 4 weeks) after birth; (2) structural images showed no clinical concerns when evaluated by a perinatal neuroradiologist (i.e., radiology score ≤ 3); (3) ≤ 10% of scans contained excessive head movement, defined as ≥ 0.3 mm FD; (4) there was good coverage (>50% overlap) of the functional ROIs selected. Among them, 12 neonates were born pre-term (birth age range: 31.7–36.9 weeks), while the remaining 106 participants were born full-term. The dHCP was approved by the UK health Research Authority. Informed parental consent was obtained for imaging acquisition and data release.

Adolescent and adult macaques (macaca mulatta).—Macaque imaging data were obtained from the PRIMatE Data Exchange (PRIME-DE) consortium (Milham et al., 2018, http://fcon_1000.projects.nitrc.org/indi/indiPRIME.html). Two cohorts of macaques were included in the present study. One of them was *Newcastle data*, where macaques were *awake* during resting-state image acquisition. Resting-state fMRI images were available for 10 macaques (Baumann et al., 2015, 2011; Poirier et al., 2017; Rinne et al., 2017; Schönwiesner et al., 2015; Slater et al., 2016; Wilson et al., 2015), but data from one macaque was removed due to poor coverage of the functional ROIs (<30% overlap; see 2.4 ROI selection and cross-population registration for details and Fig. S3 for replication using the same >50% exclusion criteria as the human subjects), resulting in 9 macaques (2 females, age = 8.4 ± 2.5 years, weight = 11.6 ± 3.6 kg) whose data were entered in the final analysis. The other one was *Oxford data*, where macaques were *anesthetized* during imaging data collection. The original dataset consisted of 20 rhesus macaque monkeys (Noonan et al., 2014). However, data of four macaques were excluded due to poor normalizations (n = 1) or insufficient coverage of functional ROIs (<30% overlap; n = 3), resulting in a final set of 16 macaques (all males, age = 3.7 ± 0.69 years, weight = 5.9 ± 1.4 kg). Together, there were 25 macaques (n = 25, mean age = 5.4 ± 2.7 years, range 2.4–13.1) whose fMRI images were included in the current study (see Table S1 for the full list of subject IDs).

2.2. Image acquisition

Human adults.—Images were collected using a 3T Siemens Skyra magnetic resonance scanner with a 32-channel head coil (Van Essen et al., 2013). Resting-state images were collected while participants fixated (eyes open) on a bright cross-hair projected on a dark background (and presented in a darkened room). A gradient-echo echo planar imaging (GE-EPI) sequence was applied with the following parameters: repetition time (TR) = 720 ms, echo time (TE) = 33.1 ms, flip angle (FA) = 52°, bandwidth = 2290 Hz/pixel, field of view (FOV) = 208 × 180 mm^2 , matrix = 104 × 90, voxel size = 2 × 2 × 2 mm^3 , multi-band (MB) factor = 8, slices = 72, and total scan time of 1200 frames = 14.6 min (Smith et al., 2013). Two sessions (i.e. REST1 and REST2) were collected on two consecutive days, each including two runs with both phase encoding directions (i.e. left-to-right and right-to-left). All four runs were used in the present study. High-resolution T1-weighted images were also acquired for all participants using a magnetized rapid gradient-echo imaging (MPRAGE) sequence with TR = 2400 ms, TE = 2.14 ms, reversal time (TI) = 1000 ms, FA = 8°, FOV = 224 × 224 mm^2, voxel size = 0.7 mm isotropic, and total scan time = 7.7 min.

Human neonates.—Images were collected using a 3T Philips Achieva with a dedicated neonatal imaging system, including a neonatal 32-channel phased array head coil (Hughes et al., 2017). All neonates were scanned during natural sleep without sedation. A multiband EPI sequence was utilized with TR = 392 ms, TE = 38ms, FA = 34°, voxel size = 2.15 × 2.15 × 2.15 mm^3, MB factor = 9, and total scan time = 2300 volume (15.05 min). T2-weighted (TR = 12 s; TE = 156 ms; sensitivity encoding (SENSE) factor: axial = 2.11, sagittal = 2.58) and inversion recovery T1-weighted (TR = 4795 ms; TI = 1740 ms; TE = 8.7 ms; SENSE factor: axial = 2.26, sagittal = 2.66) multi-slice fast spin-echo images were also collected for all neonates (in-plane resolution = 0.8 × 0.8 mm^2, 1.6 mm slices overlapped by 0.8 mm, see details in Fitzgibbon et al. (2020).

Macaque monkeys (macaca mulatta).—The *Newcastle data* were collected on a Vertical Bruker 4.7T primate dedicated scanner with a single channel or a 4–8 channel parallel imaging coil. All monkeys included in the current study were awake during resting-state imaging acquisition. Two resting-state sessions were collected for each monkey with 1.2 × 1.2 × 1.2 mm^3 resolution, TR = 2600 ms, TE = 17 ms, 10.8 min (250 volumes) per scan. T1-weighted images were also acquired using a modified driven equilibrium Fourier transform (MDEFT) sequence with the following parameters: TR = 750 ms, TE = 6ms, inversion delay = 700 ms, FOV = 12.8 × 9.6 cm^2 on a grid of 256 × 192 voxels, voxel size = 0.5 × 0.5 × 2 mm, number of slices = 22. Additionally, no contrast agent was used during scanning.

The *Oxford data* were collected on a 3T scanner with a 4-channel coil when macaques were under anesthesia. Again, no contrast agent was used. The acquisition parameters for the resting-state images were 2 × 2 × 2 mm^3 resolution, TR = 2s, TE =19 ms, FA = 90°, and total scan time = 53.3 min (1600 volumes). T1-weighted images for all monkeys were also acquired using a MPRAGE sequence with the following parameters: TR = 2500 ms, TE = 4.01ms, TI = 1100 ms, FA = 8°, voxel size = 0.5 × 0.5 × 0.5 mm.

2.3. Image preprocessing

Human adults.—We used the HCP's minimally preprocessed resting-state data (Glasser et al., 2013), which were distortion and motion corrected and registered to MNI templates via structural images using non-linear transformations. These images were further denoised using independent component analysis (ICA) with the FMRIB's ICA-based X-noiseifier (FIX) tool (Salimi-Khorshidi et al., 2014) to effectively identify and remove the components of spatiotemporal signals caused by non-neuronal or structural noise, including head movement (Smith et al., 2013). Moreover, volumes with ≥ 0.3 mm FD (Power et al., 2012) were identified as outlier scans with excessive motion. All human adults included in the current analyses had no more than 10% outliers (2.7% ± 0.025). Preprocessing procedures subsequently performed using the DPABI toolbox (Yan et al., 2016) included: (1) linear detrending to minimize the effects of low-frequency drift; (2) regression of nuisance variables, including the mean white matter (WM) and the cerebrospinal fluid (CSF) signals, continuous head movement (Friston-24 parameters, i.e., models of motion including 6 head motion parameters, 6 head motion parameters one time point before, and the 12 corresponding squared items, Friston et al., 1996) and outlier scans, to further reduce non-neuronal contributions, (3) temporal band-pass (0.01–0.1 Hz) filtering to decrease non-neurophysiological noise, and (4) spatial smoothing (Gaussian filter, FWHM = 6 mm).

Human neonates.—Similar to the HCP dataset, the resting-state functional images of the neonates first underwent a minimally preprocessed pipeline developed by the dHCP team specifically for this age range (Fitzgibbon et al., 2020). This pipeline included motion and distortion correction, registration of the functional images with corresponding T2-weighted images, as well as ICA-FIX denoising. Deformational matrices for aligning individual structural images in native space to a 40-week T2 template were also generated, and subsequently applied to the minimally preprocessed functional images to normalize them to the 40-week standard space. Images with excessive motion, defined as ≥ 0.3 mm FD, were identified and all neonates included in the current analyses had fewer than 10% of outliers (5.1% ± 0.028). Similar to the human adults, the images of the neonates were subsequently preprocessed using the DPABI toolbox for linear detrending, removal of nuisance effects (mean WM and CSF time series, Friston-24 parameters and outlier scans), temporal band-pass filtering (0.01-0.1Hz), and spatial smoothing (Gaussian filter, FWHM = 6 mm).

Macaque monkeys.—Images of both awake (*Newcastle data*) and anesthetized (*Oxford data*) monkeys were fully preprocessed using the DPABI toolbox with the following steps: (1) discarding the first five time points for signal equilibrium and adaptation to the scanning noise (this was not done for the human data because the downloaded images were already minimally preprocessed), (2) correcting for head movement, (3) removing the signal trend linearly, (4) identifying outliers defined as ≥ 0.3 mm FD, (5) normalizing to the 112RM-SL template (the volume-based atlas, McLaren et al. (2009,2010)) using unified segmentation on T1-weighted images, (6) regressing out the nuisance variables, including the mean WM and CSF time series, Friston-24 parameters and outlier scans, (7) band-pass (0.01–0.1 Hz) filtering, and (8) spatial smoothing (Gaussian filter, FWHM = 3 mm; a smaller FWHM was used here compared to that for humans because the acquisition voxel size was smaller in the awake macaque group). The anesthetized macaques showed minimal head movement during

scanning with no outlier images. The awake macaques showed a variable number of outlier images (3%-29%, mean = 13% ± 0.11) with four macaques having more than 10% of outlier images. Due to the small sample of awake macaques, their images were still included in the current study. Nevertheless, main results obtained based on the whole macaque group were replicated in awake and anesthetized macaques separately, ensuring the reliability of the current findings (Figs. S1 and S2).

2.4. ROI selection and cross-population registration (Fig. 1A)

Nodes (ROIs) of the neural networks underlying tool (and face as a control domain) processing in human adults were objectively generated from meta-analyses based on the Neurosynth database incorporating 14,371 fMRI studies in total (https://neurosynth.org, version 0.7 released July, 2018, Yarkoni et al., 2011). Association maps based on the terms “tools” and “face” were generated respectively using the default threshold at false discovery rate (FDR) corrected, $p < 0.01$ with $k = 50$ voxels.

The tool processing network, derived from 115 studies, contained three regions in the left hemisphere: left lateral occipitotemporal cortex (LOTC), left inferior frontal gyrus (LIFG), and left inferior and superior parietal lobule (LIPL/SPL). Given the frequently reported involvement of the left premotor area (LPreG) in tool-relevant tasks (Brandi et al., 2014; Lewis, 2006), including simply viewing (Chao and Martin, 2000), an additional ROI located in the LPreG was further obtained using a lenient threshold at $z = 3.09$. Note that the specific roles in tool processing for these regions are not without controversy. For instance, the LIFG cluster has been shown to activate during multiple tasks such as viewing tools, pantomiming tool use, and imaging tool use (Lewis, 2006), and hypothesized to play important roles in the neural representation of the action kinematics (Buxbaum et al., 2014), action selection/planning processes critical for tool use (Randerath et al., 2010), and/or semantic processing more generally (Carota et al., 2017). This approach, based on Neurosynth, allows to cover the brain regions supporting broad processes involved in tool understanding and use (e.g., perception, manipulation, function, semantics), which, as a network, is our question of interest.

The face processing network was derived from 896 studies and initially revealed five cerebral ROIs, including left superior temporal gyrus (LSTG), right inferior frontal (RIFG), and three large clusters in the left ($k = 3229$ voxels) and right ($k = 4728$ voxels) ventral visual pathways, as well as the right anterior temporal lobe (RATL), which extended into the subcortical areas ($k = 1156$ voxels). For the two clusters in the ventral visual pathways, more stringent thresholds were applied to identify functionally distinctive ROIs, resulting in right fusiform face area (RFFA), right occipital face area (ROFA) and right superior temporal gyrus (RSTG) on the right ($z = 5$ for RSTG; z = 11 for ROFA and RFFA) and left fusiform face area (LFFA) and left occipital face area (LOFA) on the left ($z = 8$). The stricter threshold ($z = 5$) also helped to confine the RATL to the cerebral cortex. Overall, we identified a left-hemispheric tool network and a bilateral face network (Fig. 1A, Table S2) that contained key regions commonly reported in previous meta-analyses and review papers (Lewis, 2006; Wang et al., 2020).

For neonates, these tool and face processing ROIs identified in human adults in MNI152 space were then transformed onto 40-week templates available on the dHCP- website (https://gin.g-node.org/BioMedIA/dhcp-volumetric-atlas-groupwise), using Advanced Normalization Tools (ANTs, Avants et al., 2009, https://stnava.github.io/ANTs, Fig. 1A). Hereafter, the transformed ROIs were referred to as tool (or face) homologous nodes or regions, emphasizing that they are brain regions homologous to those showing tool processing sensitivity in human adults, and not directly functionally defined in human neonates (and macaques).

For macaques, registration of the ROIs was achieved using the landmark-based functional connectivity approach recently developed by Xu et al. (2020) . Specifically, volumetric ROIs identified in human adults for tool and face processing were first mapped onto a standard surface (i.e., 32k_fs_LR) using the registration fusion approach in ANTs (RF-ANTs, Wu et al., 2018). They were then transferred from the human surface to the macaque space (Yerkes 19 atlases, Donahue et al., 2016) using a joint-embedding technique. This approach represents the functional organization of macaques and humans in a high-dimensional common space which enables establishing the cortical transformation between these two species (Xu et al., 2020). The transformed ROIs, now in macaque surface space, were then converted into volumetric space using the HCP workbench command (label-to-volume-mapping, ribbon constrained mapping algorithm) and registered to the volume-based 112RM-SL template (DPABI defaults, McLaren et al., 2009, 2010) using ANTs.

Finally, we checked whether the individual images had optimal coverage of the selected ROIs. A binary brain mask was generated based on the preprocessed functional images of each participant using the DPABI automask function, and the overlap between such binary mask and each selected ROI was calculated, as an indication of ROI coverage. All human adults and neonates met the inclusion criteria (> 50% overlap, see 2.1 Participants), showing optimal coverage of each ROI (overlap: human adults: 96% ± 0.06, human neonates: 96% ± 0.09). Note that a lenient inclusion threshold (> 30%) was applied to the macaque groups to maximize the sample sizes, which still resulted in overall good coverage (awake: 1 excluded, remaining 95% ± 0.12; anesthetized, 3 excluded, remaining: 96% ± 0.13). Replication analyses were performed based on the data of 17 macaques using the same inclusion criterion as humans (> 50%), which did not alter the main result patterns (Fig. S3).

2.5. Resting-state functional connectivity (rsFC) analyses

For each individual from all the three groups (i.e. human adults, human neonates, and macaques), the node-based timecourse was calculated by averaging across all voxels included in each ROI. Pearson correlations were then performed on the node-based timecourse for each ROI pair and the resulting correlation coefficients were transformed to Fisher Z scores. This procedure generated an rsFC matrix for each subject. Network analyses included three major steps. First, the intrinsic tool and face processing networks were evaluated in each group by comparing the rsFC between nodes belonging to the same domain with that between nodes from different domains (Fig. 1B). To this aim, a one-way repeated measures ANOVA was first performed within each group to examine the potential differences among the three sets of rsFC: the mean rsFC of the six within-tool-domain

connections among the four tool processing nodes, the mean rsFC of the 28 within-face-domain connections (eight face processing nodes), the mean rsFC of the 32 between-domain connections each connecting one tool and one face processing node. Upon significant ANOVA effects, paired *t*-tests were then carried out to evaluate the differences between the rsFC of the within-domain connections and that of the between-domain connections for the tool and face processing networks, respectively. An intrinsic network was deemed present in a specific group if the *t*-tests revealed significantly higher within-domain than between-domain rsFC.

A set of validation analyses were subsequently performed to ensure the observed network effects were not due to potential confounding variables of nodal distance, sample size, temporal signal-to-noise ratio (tSNR), and ROI selection methods (see Supplementary Materials 1.1 and 1.2 for details).

The second analysis focused on the network topology similarity between different groups. Pearson correlations were conducted on the rsFC values across paths within the tool (or face) processing network for each subject pair across all three groups (Fig. 1C), which were converted into Fisher Z scores for significance testing. One-sample *t*-tests were applied to evaluate whether each of the between-group pattern similarities were significantly greater than 0. A one-way ANOVA analysis was then performed to evaluate whether the between-group similarities differed among the three group pairs, and post-hoc comparisons were subsequently carried out upon a significant main effect. The *r* values for the corresponding Fisher Z scores were further reported (Fig. 3C) to more transparently present the correlation magnitudes of the network topology similarity between different groups.

In the final analysis, the contribution of each node and each path to the intrinsic tool network observed in human adults and neonates was investigated. A leave-one-node/path-out approach was applied, where the comparisons of within- and between- domain rsFC were re-evaluated when one node or path was removed at a time (Fig. 1D).

The Bonferroni correction for multiple comparisons was performed for all the analyses included in the current study. The Cohen's *d* and the partial $\eta 2$ effect sizes were additionally computed for the significant *t*-test and ANOVA test results, respectively, for clearer interpretation.

3. Results

3.1. Intrinsic functional connectivity results

Human adult tool network characterization.—Using the human adult resting-state dataset available in the HCP, we demonstrated that these regions being consistently activated by tools (or faces) constituted tightly connected networks, replicating previous literature (Peelen et al., 2013; Stevens et al., 2015; Wang et al., 2016). Specifically, the ANOVA analysis revealed significant group differences ($F_{2,198} = 118.27$, $p < 0.001$, partial $\eta^2 = 0.54$) among the within-tool-domain, within-face-domain and between-domain rsFC. Post-hoc analyses further demonstrated significantly greater rsFC among the tool processing nodes and among the face processing nodes than the rsFC between tool and face processing nodes

(within-tool-domain > between-domain: t_{99} = 15.4, $p_{corrected}$ < 0.001, *Cohen's d* = 1.54; within-face-domain > between-domain: t_{99} = 15.4, $p_{corrected}$ < 0.001, *Cohen's d* = 1.54, Fig. 2A).

Tool homologous intrinsic network structure present in human neonates.— Based on the resting-state images of human neonates available from dHCP, significant differences among the within-tool-domain, within-face-domain and between-domain rsFC were first revealed by the ANOVA analysis ($F_{2,234}$ = 126.3, p < 0.001, partial η^2 = 0.52). Post-hoc analyses further demonstrated that the within-domain rsFC for the tool homologous network was significantly greater than between-domain rsFC (t_{117} = 12.4, $p_{corrected}$ < 0.001, *Cohen's d* = 1.1, Fig. 2A), suggesting the presence of an intrinsic functional network among the tool homologous regions in human neonates. The same results held when the pre-term and full-term neonates were analyzed separately (full-term neonates: t_{105} = 11.4, $p_{corrected}$ < 0.001, *Cohen's d* = 1.1; pre-term neonates: t_{11} = 6.3, $p_{corrected}$ < 0.001, *Cohen's d* = 1.8, Fig. S1A). No coherent face homologous network was observed in neonates, as within-face-domain rsFC was not stronger than between-domain rsFC (t_{117} = −4.5, $p_{corrected}$ < 0.001; i.e., in the reverse direction of the face-network presence).

Tool homologous intrinsic network structure absent in macaques.—The ANOVA analysis based on the macaque dataset available in the PRIME-DE consortium revealed a significant main effect for the differences among the within-tool-domain, within-face-domain and between-domain rsFC ($F_{2,48}$ = 22.5, p < 0.001, partial η^2 = 0.48). Post-hoc analyses showed that the within-tool-domain rsFC was not stronger than between-domain rsFC (t_{24} = −3.95, p = 0.001; i.e., in the reverse direction of the tool-network presence, Fig. 2A), indicating that the homologous regions derived from the tool processing ROIs in human adults did not form an intrinsic brain network structure in the macaque brain. In contrast, a face homologous network was observed using the same approach, as within-face-domain rsFC was significantly greater than between-domain rsFC (t_{24} = 4.5, $p_{corrected}$ < 0.001, *Cohen's d* = 0.90, Fig. 2A). The presence of the face homologous network in macaques was further replicated both in a subsample of 9 macaques who were awake during scanning (t_8 = 5.6, $p_{corrected}$ = 0.001, *Cohen's d* = 1.9) and 16 macaques who were anesthetized during imaging acquisition (t_{15} = 2.5, $p_{corrected}$ = 0.048, *Cohen's d* = 0.63, Fig. S1A).

Validation analyses controlling for nodal distance, sample size, tSNR, and ROI selection methods.—The result patterns above were robust across a series of validation analyses that controlled for potential effects of nodal distance across networks (Fig. 2B), sample size difference across groups (Fig. 2C), tSNR differences across populations (Fig. S4), and methods of ROI selection (see Supplementary Materials 1.1 and 1.2 for details).

3.2. Network topology results: Highly similar tool homologous network topology between human adults and neonates, but not between humans and macaques

In addition to the network-level rsFC analyses above, we further characterized and compared every network connection among the tool processing nodes (or their homologues) across the three population groups. Fig. 3A visualizes the topological pattern of the tool (homologous) network for each group by showing the path-wise rsFC strengths. The stronger similarity

between the human adult and human neonate groups shown in the figure was further confirmed by the topological similarity results on the tool (homologous) processing network (see Fig. 1C for the method and Fig. 3B for the cross-subject correlation matrix across all subjects). Specifically, the topological patterns of the tool (homologous) networks in human adults and neonates were significantly correlated with large effect sizes (r = 0.52 ± 0.48, one-sample t_{11799} = 119.3, $p_{corrected}$ < 0.001, *Cohen's d* = 1.1, Fig. 3C). By contrast, the similarities between the macaque group and either human group were, although statistically significant, very low (human adults-macaques: w 0.054 ± 0.49, one-sample t_{2499} = 5.1, $p_{corrected}$ < 0.001, *Cohen's d* = 0.10; human neonates-macaques, r = 0.080 ± 0.48, one-sample t_{2949} = 8.4, $p_{corrected}$ < 0.001, *Cohen's d* = 0.15, Fig. 3C). The ANOVA analysis on the between-group similarities among the three group pairs further revealed a significant main effect $F_{2,17247}$ = 1742.8, p < 0.001, partial η^2 = 0.17). Post-hoc analyses showed that the similarity between the two human groups was significantly higher than each of the between-species similarities (human adults-human neonates vs. human adults-macaques: t_{14298} = 45.0, $p_{corrected}$ < 0.001, *Cohen's d* = 0.99; human adults-human neonates vs. human neonates-macaque: t_{14748} = 46.0, $p_{corrected}$ < 0.001, *Cohen's d* = 0.95, Fig. 3C), while the latter two did not differ significantly from each other (t_{5448} = 1.8, p = 0.07).

To deal with the limited number of connections (n=6) in the tool processing network that might impact the topological similarity results, a validation analysis was conducted, in which the time series of each participant was split into 10 bins, resulting in 60 data points per subjects for the topological similarity computation. This validation analysis revealed the same result pattern as reported here (see Supplementary Materials 1.3 for details).

For the face homologous network, all between-group correlations for the face (homologous) network were significant with large or medium effect sizes (human adults-neonates: r = 0.51 ± 0.26, one-sample t_{11799} = 234.0, $p_{corrected}$ < 0.001, *Cohen's d* = 2.2; human adults-macaques: r = 0.47 ± 0.21, one-sample t_{2499} = 116.7, $p_{corrected}$ < 0.001, *Cohen's d* = 2.3; human neonates-macaques, r = 0.43 ± 0.25, one-sample t_{2949} = 100.0, $p_{corrected}$ < 0.001, *Cohen's d* = 1.8, Fig. S5). The ANOVA analysis demonstrated significant group differences in the between-group similarities among the three group pairs ($F_{2,17247}$ = 229.9, p < 0.001, partial η^2 = 0.03). Post-hoc analyses showed that the topological patterns for the face (homologous) network were more similar between human adults and neonates than between human adults and macaques (t_{14298} = 11.1, $p_{corrected}$ < 0.001, *Cohen's d* = 0.25), which were in turn were more similar than those between human neonates and macaques (t_{5448} = 6.6, $p_{corrected}$ < 0.001, *Cohen's d* = 0.18, Fig. S5). The network topology results mostly remained for both the tool and face processing networks when pre-term and full-term neonates and when awake and anesthetized macaques were analyzed separately (Fig. S2).

3.3. Nodal and path results: Strong contributions of premotor connectivity to the formation of the intrinsic tool homologous network in human neonates

Is the formation of the tool (homologous) network in human adults and neonates driven by any particular region(s) or functional connection(s)? This question was addressed using leave-one-node/path-out analyses (Fig. 1D). In human adults, when any single node/path was removed, the remaining network still showed stronger within- than between-domain

rsFC (all $ts > 5$, all $p_{corrected} < 0.001$, Fig. S6A), suggesting that the tool processing network was robust in human adults (see the same result patterns derived from the left-hemispheric nodes in Fig. S6B). By contrast, in human neonates, when the left premotor node was removed, the remaining tool processing nodes no longer formed an intrinsic network ($t_{117} = 1.2$, $p = 0.24$). Removal of any other node or path did not affect the presence of the tool homologous network (i.e., within-tool-domain - between-domain rsFC > 0, all $ts > 4$, all $p_{corrected} < 0.001$, Fig. 4A). Furthermore, the same analyses were repeated using only the left-hemispheric nodes, to ensure balanced within-tool-domain and between-domain nodal distances. All results were replicated except that the removal of the left inferior/superior parietal node or its connection with the left premotor node made the tool homologous network no longer observable (node removal results: $t_{117} = 0.24$, $p = 0.81$; path removal results: $t_{117} = 1.9$, $p = 0.06$, Fig. 4B). That is, the connection between left premotor and left inferior/superior parietal nodes (LPreG-LIPL/SPL) is particularly important for the presence of the intrinsic tool homologous network at birth in humans (see replication of the results for nodal and path contributions in subsamples of pre-term and full-term neonates in Fig. S7).

The path results were further corroborated by the direct group comparisons on the rsFC of each path, as visualized in Fig. 3A. The LPreG-LIPL/SPL connection was the most comparable between human adults and neonates, with smallest t value in two-sample comparisons between human adults and neonates (Table S3) and significantly lower rsFC differences when compared with most of other paths (Table S4). Meanwhile, this LPreG-LIPL/SPL connection also revealed the strongest differences between human neonates and macaques (Fig. 3A), with the largest t value in two-sample comparisons (Table S3) and significant group x path interaction effects when contrasted with other paths (Table S4). In addition, while the LPreG was significantly connected to the LIPL/SPL in both human adults and neonates ($ts > 5$, $p_{corrected} < 0.001$), this connection was not significantly above zero in the macaque brain ($t_{24} = 1.54$, $p = 0.14$), further suggesting the species-specific nature of this path.

4. Discussion

To test whether the intrinsic brain connectivity structure supporting tool processing observed in human adults is driven by individual object manipulation experience or is predisposed in humans, we compared their resting-state functional connectivity (rsFC) in this network to homologous networks in human neonates (without manipulation experience) and mature/adolescence macaques (with motor experience with objects), using face (homologous) networks as references. We found that the brain regions that are homologous to those supporting tool processing in human adults were more strongly intrinsically connected with each other than with other nodes (face homologous regions) in the human neonate brain, thereby forming an intrinsic functional network. The homologous regions in macaques did not, however, show a greater within-tool-domain rsFC when compared to the between-domain connectivity. The overall topological patterns among these regions were also highly similar between human adults and human neonates, and much less similar between humans and macaques. The left premotor region, especially its functional connection with the parietal cortex, was particularly important in the formation of the tool homologous network in human neonates.

It should first be acknowledged that the nodes evaluated in human neonate and macaque brains were transformed from regions-of-interest defined in human adult brains using advanced registration methods, including the recently developed cross-species functional alignment approach (Xu et al., 2020) and tools offered by ANTs (Avants et al., 2009). The transformation to neonates' and other species' brains is not a trivial task, and is more than a technical challenge. Precise transformation applies if a structure is fully conservative – having the same anatomical and functional correspondence across species (and developmental stage for the case of neonate-adult comparison), which is actually exactly the question at stake here – to what extent the brain system supporting tools is conservative across species and/or "innate" in humans. The approach taken here is to use the state-of-art transformation approach for each population of interest, and the same approach for regions/networks of interest (tool cognition) and for regions that previously have shown to be relatively conservative (as control; face regions). The cross-species functional alignment approach we adopted here uses a joint-embedding technique that represents the functional organization of human and macaque brains in a high-dimensional common space. This method allows for cortical transformation between species, which had been suggested as the state-of-art transformation approach (Liu et al., 2021; Van Essen et al., 2019). The face homologous nodes in the macaque brain obtained using this transformation approach were largely consistent with those identified based on task-based fMRI studies in macaques (Hesse and Tsao, 2020; Ku et al., 2011; Landi and Freiwald, 2017; Tsao et al., 2008). The observation of the significant similarity of the face network between macaques and humans, and not the tool network derived from the same transformation approach, suggests the "human tool network" was not as conservative. Furthermore, convergence was also obtained using ROIs derived from the anatomically-defined atlas available for each population that approximated the functional ROIs, which, although less precise, circumvent the transformation processes (Supplementary Materials 1.2). These different types of cross-species brain mapping rely on different sets of assumptions, and the convergence across different approaches increases the confidence of the findings.

Our main observations were that the tool homologous network is present in human neonates, but not significantly identified in macaques, and that the intrinsic functional connectivity pattern of this network is more similar between human adults and human neonates than between human adults and macaques. This composite pattern suggests that the tool processing network may be (at least partly) specific to humans, and is in place early in human development. This network is not (fully) driven by simple sensorimotor experiences per se, as for human neonates, the voluntary grasping is not developed until 2–6 months old (Touwen, 1995), let alone to manipulate tools. By contrast, although there are no documented data on object interaction experiences of the macaques in the current dataset, they were mature or adolescent in age, typically with developed sensorimotor skills at least for grasping objects such as food. Worth emphasizing is that we are not claiming that this network is not associated with sensorimotor experience at all. In human adults, the tool processing network showed robust within- than between-domain rsFC after the removal of any node or path, revealing that the tool network effect in human adults is not driven by any single node/path but rather is a composite pattern where the overall connectivity is tight to support tool use. Moreover, the functional connectivity for the tool processing network

tended to be stronger for human adults than for neonates, indicating the sculpting effects of postnatal experiences. Nevertheless, the developmental changes of the tool network are not at odds with its presence in neonates, as the latter suggests that sensorimotor experiences, at least in primary forms such as grasping, are not fully necessary (in neonates) or sufficient (in macaques) for this network structure to emerge at the first place.

In macaques, a brain network supporting hand grasping abilities has been identified, including AIP, F5, m12r/m46v, and TEa/m (Borra et al., 2017; Howells et al., 2020; Premereur et al., 2015). The tool homologous network discussed here partly overlaps with this grasping network (Fig. S8) and their relationship is worth specific discussion. Cognitively, tool processing in humans certainly involves grasping, but goes beyond simple grasping an object and entails an understanding of how to manipulate it in a way appropriate for functional use, based on the causal/mechanical relationship between its physical properties, use, and function (e.g., Watson and Buxbaum 2015). Neurally, various kinds of properties about tools such as shape, grasping, and manipulation knowledge, are preferentially represented by different brain regions in the human adult brain (e.g., parietal cluster for shape/grasping/manipulation; frontal cluster for manipulation; see e.g., Wang et al. 2018, Wu et al. 2020). Species differences were observed in the left inferior parietal cortex, with IPL typically being activated during tool activity viewing in humans and not macaques (Kastner et al., 2017; Peeters et al., 2009), and showing significant differences between humans and macaques in terms of anatomical (Cheng et al., 2021) and functional connectivity patterns (Xu et al., 2020). Aligning with these previous findings, we also found that the functional connectivity of the parietal cluster (with premotor cluster) was most saliently different between species (humans and macaques) and similar within species (human adults and neonates).

It is thus tempting to associate the observed intrinsic functional network pattern showing species difference, the parietal-premotor connection in particular, to those cognitive components showing species difference, i.e., the causal (mechanic) understanding (as opposed to similar components such as grasping and/or simple sensorimotor associations). The current consensus from the cognitive/behavioral studies is that while macaques are capable of grasping and using simple tools based on surface property associations, they lack an understanding of the causal mechanic mechanisms related to tools and are incapable of generalizing functions of objects (Vaesen, 2012). Although numerous studies have reported the ability to learn tool-use behaviors in captive macaques, trained macaques still differ from human adults in tool use behavior (i.e., causal reasoning behavior, Johnson-Frey, 2003; Visalberghi and Limongelli, 1994) and neural activities (Peeters et al., 2009). This speculation is also in line with the contemporaneous emergence of flexible tool use behaviors and perceptual and motor skills at early developmental stages (Kastner et al., 2017), and with lesion studies in human adults, which showed significant associations between damage to parietal-premotor white matter connections and difficulty understanding and using tools (Bi et al., 2015). However, we fully acknowledge that this speculation is inferred by bridging several separate lines of evidence, and further studies are invited to directly assess this hypothesis, to elucidate whether the tool network emerges from networks of prerequisite cognitive processes such as the grasping network, whether and to what extent the development of tool use and training with tools may modulate the tool

processing network, and the white matter structural connectivity in human neonates and nonhuman primates. The rsFC findings in the present study are well-suited to guide such future studies, given the tight coupling between neural connectivity and function (Mars et al., 2018; Passingham et al., 2002).

For human neonates, the functionality and connectivity patterns of regions that become tool-sensitive were poorly understood. To date, most studies investigating rsFC in infants have focused on primary (e.g., sensorimotor and visual) functional networks and higher-order functional networks underlying domain-general cognition (Gilmore et al., 2018), and have reported protracted maturation of the default-mode and attention networks such that they do not reach adult-like topology until age two (Fiske and Holmboe, 2019; Gao et al., 2015). More broadly, the identified large-scale brain networks in infancy using parcellation approaches do not correspond well with the tool homologous network we observed here (Doria et al., 2010; Fransson et al., 2007; Gao et al., 2015, except for Fitzgibbon et al. (2020) , in which one of the 16 subnetworks is visually similar). Thus, the tool network studied here is not to be explained by those broader networks such as the somatosensory and visual attention networks. The results for the face homologous network in human neonates are worth further discussion. While the overall network topology among the face (homologous) nodes was significantly similar between human adults and neonates, more so than that between human and macaque species, we did not observe a robust intrinsic face homologous network based on within-face-domain versus between-domain comparisons. That is, on the whole brain level the face homologous regions were not robustly segregated from the tool homologous nodes in neonates. Previous studies focusing on the visual cortex have reported the emergence of adult-like face-relevant profiles in human neonates/infants. Specifically, similar to adults, intrinsic functional connections among the homologues of occipital face areas, fusiform face areas, and foveal V1 areas were observed in neonates (Kamps et al., 2020). Moreover, face-preferring topography present in the ventral visual cortex of adults during face-viewing were similarly observed in infants 4-6 months of age (Deen et al., 2017). Together, these results suggest that while the intrinsic functional wiring potentially supporting face processing within the visual cortex is at least partly present at birth, the large-scale functional network associated with adult face recognition, especially beyond the visual cortex, is under-developed (see also Arcaro et al. 2017). Consistent with this interpretation, we also found that the OFA-FFA connectivity (i.e. mean rsFC of the LFFA-LOFA and RFFA-ROFA connections) was stronger than the intra-hemispheric connectivity between OFA/FFA and ROIs outside the visual pathway cortex (i.e. mean rsFC of the LFFA-LSTG, LOFA-LSTG, RFFA-RSTG, RFFA-RATL, RFFA-RIFG, ROFA-RSTG, ROFA-RATL, and ROFA-RIFG connections, $t_{117} = 21.6$, $p < 0.001$, *Cohen's d* = 2.0).

To conclude, for the brain network supporting tool processing in human adults, the intrinsic functional connectivity network structure is absent among the homologous regions in our evolutionary cousins, macaque monkeys, but is present in humans at birth before they have had individual experiences interacting with objects. The functional connection between premotor and parietal nodes, in particular, is important for the formation of the tool homologous network connectivity in human neonates and thereby constitutes a strong candidate for the neural basis of complex tool use specific to humans. These results contribute empirical evidence to the broad issue of which neural aspects are human specific,

and highlight the need for further research to understand the neural and computational underpinnings of tool use.

Supplementary Material

Refer to Web version on PubMed Central for supplementary material.

Acknowledgments

This work was supported by the National Science and Technology Innovation 2030 Major Program (2021ZD0204104 awarded to Y.B.), the National Natural Science Foundation of China (32100867 awarded to X.Y., 31925020, 82021004 awarded to Y.B., 32071050 awarded to X.Y.W), Changjiang Scholar Professorship Award (T2016031 awarded to Y.B.), the Fundamental Research Funds for the Central Universities (awarded to X.Y., 2021NTST11 awarded to X.Y.W), and the National Institutes of Health BRAIN Initiative (RF1MH128696 awarded to T.X.). The human adult data were provided by the Human Connectome Project, WU-Minn Consortium (Principal Investigators: David Van Essen and Kamil Ugurbil; 1U54MH091657), which is funded by the 16 NIH Institutes and Centers that support the NIH Blueprint for Neuroscience Research; and by the McDonnell Center for Systems Neuroscience at Washington University. The neonate data were provided by the developing Human Connectome Project, KCL-Imperial-Oxford Consortium, which is funded by the European Research Council under the European Union Seventh Framework Programme (FP/2007-2013) / ERC Grant Agreement no. [319456]. The macaque data were provided by investigative teams from Oxford (Principal Investigators: Jerome Sallet, Rogier B. Mars, Matthew F.S. Rushworth) and funded by the Wellcome Trust, Royal Society, Medical Research Council UK and the Biotechnology and Biological Sciences Research Council UK, and the teams from Newcastle (Principal Investigators: Jennifer Nacef, Christopher I. Petkov, Fabien Balezeau, Timothy D. Griffiths, Colline Poirier, Alexander Thiele, Michael Ortiz, Michael Schmid, David Hunter), which are funded by the Wellcome Trust, National Center for 3Rs, UK Biotechnology and Biological Sciences Research Council and National Institutes of Health. We would like to thank the investigative teams providing these publicly available datasets and the funding agencies that make these datasets available. We would also like to acknowledge the assistance of Yaya Jiang, Yumeng Xin and Xinyu Liang for constructive suggestions in data analysis, and Xinyi Tang for helpful comments on earlier drafts of the manuscript.

References

Ambrose SH, 2001. Paleolithic technology and human evolution. Science 291, 1748–1753. doi:10.1126/science.1059487. [PubMed: 11249821]

Arcaro MJ, Schade PF, Vincent JL, Ponce CR, Livingstone MS, 2017. Seeing faces is necessary for face-domain formation. Nat. Neurosci 20, 1404–1412. doi:10.1038/nn.4635. [PubMed: 28869581]

Avants BB, Tustison N, Song G, 2009. Advanced normalization tools (ANTS). Insight J. 2, 1–35.

Baumann S, Griffiths TD, Sun L, Petkov CI, Thiele A, Rees A, 2011. Orthogonal representation of sound dimensions in the primate midbrain. Nat. Neurosci 14, 423–425. doi:10.1038/nn.2771. [PubMed: 21378972]

Baumann S, Joly O, Rees A, Petkov CI, Sun L, Thiele A, Griffiths TD, 2015. The topography of frequency and time representation in primate auditory cortices. eLife 4, e03256. doi:10.7554/eLife.03256.

Bentley-Condit V, Smith, 2010. Animal tool use: current definitions and an updated comprehensive catalog. Behaviour 147, 185. doi:10.1163/000579509X12512865686555, −32A.

Bi Y, Han Z, Zhong S, Ma Y, Gong G, Huang R, Song L, Fang Y, He Y, Caramazza A, 2015. The white matter structural network underlying human tool use and tool understanding. J. Neurosci 35, 6822–6835. doi:10.1523/JNEUROSCI.3709-14.2015. [PubMed: 25926458]

Bi Y, Wang X, Caramazza A, 2016. Object Domain and Modality in the Ventral Visual Pathway. Trends Cogn. Sci 20 (4), 282–290. doi:10.1016/j.tics.2016.02.002. [PubMed: 26944219]

Borra E, Gerbella M, Rozzi S, Luppino G, 2017. The macaque lateral grasping network: a neural substrate for generating purposeful hand actions. Neurosci. Biobehav. Rev 75, 65–90. doi:10.1016/j.neubiorev.2017.01.017. [PubMed: 28108414]

Brandi ML, Wohlschlager A, Sorg C, Hermsdorfer J, 2014. The neural correlates of planning and executing actual tool use. J. Neurosci 34, 13183–13194. doi:10.1523/JNEUROSCI.0597-14.2014. [PubMed: 25253863]

Buxbaum LJ, Shapiro AD, Coslett HB, 2014. Critical brain regions for tool-related and imitative actions: a componential analysis. Brain 137, 1971–1985. doi:10.1093/brain/awu111. [PubMed: 24776969]

Carota F, Kriegeskorte N, Nili H, Pulvermüller F, 2017. Representational similarity mapping of distributional semantics in left inferior frontal, middle temporal, and motor cortex. Cereb. Cortex doi:10.1093/cercor/bhw379, cercor;bhw379v1.

Chao LL, Martin A, 2000. Representation of manipulable man-made objects in the dorsal stream. Neuroimage 12, 478–484. doi:10.1006/nimg.2000.0635. [PubMed: 10988041]

Cheng L, Zhang Y, Li G, Wang J, Sherwood C, Gong G, Fan L, Jiang T, 2021. Connectional asymmetry of the inferior parietal lobule shapes hemispheric specialization in humans, chimpanzees, and rhesus macaques. eLife 10, e67600. doi:10.7554/eLife.67600. [PubMed: 34219649]

Chouinard PA, Goodale MA, 2012. FMRI-adaptation to highly-rendered color photographs of animals and manipulable artifacts during a classification task. Neuroimage 59, 2941–2951. doi:10.1016/j.neuroimage.2011.09.073. [PubMed: 22015854]

Deen B, Richardson H, Dilks DD, Takahashi A, Keil B, Wald LL, Kanwisher N, Saxe R, 2017. Organization of high-level visual cortex in human infants. Nat. Commun 8, 13995. doi:10.1038/ncomms13995. [PubMed: 28072399]

Donahue CJ, Sotiropoulos SN, Jbabdi S, Hernandez-Fernandez M, Behrens TE, Dyrby TB, Coalson T, Kennedy H, Knoblauch K, Van Essen DC, Glasser MF, 2016. Using diffusion tractography to predict cortical connection strength and distance: a quantitative comparison with tracers in the Monkey. J. Neurosci 36, 6758–6770. doi:10.1523/JNEUROSCI.0493-16.2016. [PubMed: 27335406]

Doria V, Beckmann CF, Arichi T, Merchant N, Groppo M, Turkheimer FE, Counsell SJ, Murgasova M, Aljabar P, Nunes RG, Larkman DJ, Rees G, Edwards AD, 2010. Emergence of resting state networks in the preterm human brain. Proc. Natl. Acad. Sci 107, 20015–20020. doi:10.1073/pnas.1007921107. [PubMed: 21041625]

Fayet AL, Hansen ES, Biro D, 2020. Evidence of tool use in a seabird. Proc. Natl. Acad. Sci 117, 1277–1279. doi:10.1073/pnas.1918060117. [PubMed: 31889002]

Fiske A, Holmboe K, 2019. Neural substrates of early executive function development. Dev. Rev 52, 42–62. doi:10.1016/j.dr.2019.100866. [PubMed: 31417205]

Fitzgibbon SP, Harrison SJ, Jenkinson M, Baxter L, Robinson EC, Bastiani M, Bozek J, Karolis V, Cordero Grande L, Price AN, Hughes E, Makropoulos A, Passerat-Palmbach J, Schuh A, Gao J, Farahibozorg SR, O'Muircheartaigh J, Ciarrusta J, O'Keeffe C, Brandon J, Arichi T, Rueckert D, Hajnal JV, Edwards AD, Smith SM, Duff E, Andersson J, 2020. The developing human connectome project (dHCP) automated resting-state functional processing framework for newborn infants. Neuroimage 223, 117303. doi:10.1016/j.neuroimage.2020.117303. [PubMed: 32866666]

Fransson P, Skio B, Horsch S, Nordell A, Blennow M, Lagercrantz H, Åden U, 2007. Resting-state networks in the infant brain. Proc. Natl. Acad. Sci 104, 15531–15536. [PubMed: 17878310]

Friston KJ, Williams S, Howard R, Frackowiak RSJ, Turner R, 1996. Movement-related effects in fMRI time-series: movement artifacts in fMRI. Magn. Reson. Med 35, 346–355. doi:10.1002/mrm.1910350312. [PubMed: 8699946]

Gao W, Alcauter S, Elton A, Hernandez-Castillo CR, Smith JK, Ramirez J, Lin W, 2015. Functional network development during the first year: relative sequence and socioeconomic correlations. Cereb. Cortex 25, 2919–2928. doi:10.1093/cercor/bhu088. [PubMed: 24812084]

Garcea FE, Greene C, Grafton ST, Buxbaum LJ, 2020. Structural disconnection of the tool use network after left hemisphere stroke predicts limb apraxia severity. Cereb. Cortex Commun 1, 1–20. doi:10.1093/texcom/tgaa035.

Gibson KR, Gibson KR, Ingold T, 1994. Tools, Language and Cognition in Human Evolution. Cambridge University Press.

Gilmore JH, Knickmeyer RC, Gao W, 2018. Imaging structural and functional brain development in early childhood. Nat. Rev. Neurosci 19, 123–137. doi:10.1038/nrn.2018.1. [PubMed: 29449712]

Glasser MF, Sotiropoulos SN, Wilson JA, Coalson TS, Fischl B, Andersson JL, Xu J, Jbabdi S, Webster M, Polimeni JR, Van Essen DC, Jenkinson M, 2013. The minimal

preprocessing pipelines for the human connectome project. Neuroimage 80, 105–124. doi:10.1016/j.neuroimage.2013.04.127. [PubMed: 23668970]

Hesse JK, Tsao DY, 2020. The macaque face patch system: a turtle's underbelly for the brain. Nat. Rev. Neurosci 21, 695–716. doi:10.1038/s41583-020-00393-w. [PubMed: 33144718]

Howells H, Simone L, Borra E, Fornia L, Cerri G, Luppino G, 2020. Reproducing macaque lateral grasping and oculomotor networks using resting state functional connectivity and diffusion tractography. Brain Struct. Funct 225, 2533–2551. doi:10.1007/s00429-020-02142-2. [PubMed: 32936342]

Hughes EJ, Winchman T, Padormo F, Teixeira R, Wurie J, Sharma M, Fox M, Hutter J, Cordero-Grande L, Price AN, Allsop J, Bueno-Conde J, Tusor N, Arichi T, Edwards AD, Rutherford MA, Counsell SJ, Hajnal JV, 2017. A dedicated neonatal brain imaging system: a dedicated neonatal brain imaging system. Magn. Reson. Med 78, 794–804. doi:10.1002/mrm.26462. [PubMed: 27643791]

Johnson-Frey SH, 2003. What's so special about human tool use? Neuron 39, 201–204. doi:10.1016/S0896-6273(03)00424-0. [PubMed: 12873378]

Kamps FS, Hendrix CL, Brennan PA, Dilks DD, 2020. Connectivity at the origins of domain specificity in the cortical face and place networks. Proc. Natl. Acad. Sci 117, 6163–6169. doi:10.1073/pnas.1911359117. [PubMed: 32123077]

Kastner S, Chen Q, Jeong SK, Mruczek REB, 2017. A brief comparative review of primate posterior parietal cortex: a novel hypothesis on the human toolmaker. Neuropsychologia 105, 123–134. doi:10.1016/j.neuropsychologia.2017.01.034. [PubMed: 28159617]

Konkle T, Caramazza A, 2017. The large-scale organization of object-responsive cortex is reflected in resting-state network architecture. Cereb. Cortex 29, 4933–4945.

Ku SP, Tolias AS, Logothetis NK, Goense J, 2011. fMRI of the face-processing network in the ventral temporal lobe of awake and anesthetized macaques. Neuron 70, 352–362. doi:10.1016/j.neuron.2011.02.048. [PubMed: 21521619]

Laland K, Seed A, 2021. Understanding human cognitive uniqueness. Annu. Rev. Psychol 72, 689–716. doi:10.1146/annurev-psych-062220-051256. [PubMed: 33400565]

Landi SM, Freiwald WA, 2017. Two areas for familiar face recognition in the primate brain. Science 357, 591–595. doi:10.1126/science.aan1139. [PubMed: 28798130]

Lewis JW, 2006. Cortical networks related to human use of tools. Neuroscientist 12, 211–231. doi:10.1177/1073858406288327. [PubMed: 16684967]

Liu X, Eickhoff SB, Caspers S, Wu J, Genon S, Hoffstaedter F, Mars RB, Sommer IE, Eickhoff CR, Chen J, Jardri R, Reetz K, Dogan I, Aleman A, Kogler L, Gruber O, Caspers J, Mathys C, Patil KR, 2021. Functional parcellation of human and macaque striatum reveals human-specific connectivity in the dorsal caudate. Neuroimage 235, 118006. doi:10.1016/j.neuroimage.2021.118006. [PubMed: 33819611]

Mahon BZ, Poeppel D, Mangun GR, Gazzaniga MS, 2020. The representation of tools in the human brain. In: The Cognitive Neuroscience. MIT Press, Cambridge, Massachusetts, pp. 765–776.

Makropoulos A, Robinson EC, Schuh A, Wright R, Fitzgibbon S, Bozek J, Counsell SJ, Steinweg J, Vecchiato K, Passerat-Palmbach J, Lenz G, Mortari F, Tenev T, Duff EP, Bastiani M, Cordero-Grande L, Hughes E, Tusor N, Tournier J-D, Hutter J, Price AN, Teixeira RPAG, Murgasova M, Victor S, Kelly C, Rutherford MA, Smith SM, Edwards AD, Hajnal JV, Jenkinson M, Rueckert D, 2018. The developing human connectome project: a minimal processing pipeline for neonatal cortical surface reconstruction. Neuroimage 173, 88–112. doi:10.1016/j.neuroimage.2018.01.054. [PubMed: 29409960]

Mars RB, Passingham RE, Jbabdi S, 2018. Connectivity fingerprints: from areal descriptions to abstract spaces. Trends Cogn. Sci 22, 1026–1037. doi:10.1016/j.tics.2018.08.009. [PubMed: 30241910]

McLaren DG, Kosmatka KJ, Kastman EK, Bendlin BB, Johnson SC, 2010. Rhesus macaque brain morphometry: a methodological comparison of voxel-wise approaches. Methods 50, 157–165. doi:10.1016/j.ymeth.2009.10.003. [PubMed: 19883763]

McLaren DG, Kosmatka KJ, Oakes TR, Kroenke CD, Kohama SG, Matochik JA, Ingram DK, Johnson SC, 2009. A population-average MRI-based atlas collection of the rhesus macaque. Neuroimage 45, 52–59. doi:10.1016/j.neuroimage.2008.10.058. [PubMed: 19059346]

Milham MP, Ai L, Koo B, Xu T, Amiez C, Balezeau F, Baxter MG, Blezer ELA, Brochier T, Chen A, Croxson PL, Damatac CG, Dehaene S, Everling S, Fair DA, Fleysher L, Freiwald W, Froudist-Walsh S, Griffiths TD, Guedj C, Hadj-Bouziane F, Ben Hamed S, Harel N, Hiba B, Jarraya B, Jung B, Kastner S, Klink PC, Kwok SC, Laland KN, Leopold DA, Lindenfors P, Mars RB, Menon RS, Messinger A, Meunier M, Mok K, Morrison JH, Nacef J, Nagy J, Rios MO, Petkov CI, Pinsk M, Poirier C, Procyk E, Rajimehr R, Reader SM, Roelfsema PR, Rudko DA, Rushworth MFS, Russ BE, Sallet J, Schmid MC, Schwiedrzik CM, Seidlitz J, Sein J, Shmuel A, Sullivan EL, Ungerleider L, Thiele A, Todorov OS, Tsao D, Wang Z, Wilson CRE, Yacoub E, Ye FQ, Zarco W, Zhou Y, Margulies DS, Schroeder CE, 2018. An open resource for non-human primate imaging. Neuron 100, 61–74. doi:10.1016/j.neuron.2018.08.039, e2.. [PubMed: 30269990]

Noonan MP, Sallet J, Mars RB, Neubert FX, O'Reilly JX, Andersson JL, Mitchell AS, Bell AH, Miller KL, Rushworth MFS, 2014. A neural circuit covarying with social hierarchy in macaques. PLoS Biol. 12, e1001940. doi:10.1371/journal.pbio.1001940. [PubMed: 25180883]

Oakley KP, 1956. Man the Tool-Maker, 3rd ed. Printed by order of the Trustees of the British Museum.

Obayashi S, Suhara T, Kawabe K, Okauchi T, Maeda J, Akine Y, Onoe H, Iriki A, 2001. Functional brain mapping of Monkey tool use. Neuroimage 14, 853–861. doi:10.1006/nimg.2001.0878. [PubMed: 11554804]

Osiurak F, Reynaud E, 2020. The elephant in the room: what matters cognitively in cumulative technological culture. Behav. Brain Sci 43, 1–66. doi:10.1017/S0140525X19003236, e156.

Passingham RE, Stephan KE, Kötter R, 2002. The anatomical basis of functional localization in the cortex. Nat. Rev. Neurosci 3, 606–616. doi:10.1038/nrn893. [PubMed: 12154362]

Peelen MV, Bracci S, Lu X, He C, Caramazza A, Bi Y, 2013. Tool selectivity in left occipitotemporal cortex develops without vision. J. Cogn. Neurosci 25, 1225–1234. doi:10.1162/jocn_a_00411. [PubMed: 23647514]

Peeters R, Simone L, Nelissen K, Fabbri-Destro M, Vanduffel W, Rizzolatti G, Orban GA, 2009. The representation of tool use in humans and Monkeys: common and uniquely human features. J. Neurosci 29, 11523–11539. doi:10.1523/JNEUROSCI.2040-09.2009. [PubMed: 19759300]

Penn DC, Holyoak KJ, Povinelli DJ, 2008. Darwin's mistake: explaining the discontinuity between human and nonhuman minds. Behav. Brain Sci 31, 109–130. doi:10.1017/S0140525X08003543. [PubMed: 18479531]

Poirier C, Baumann S, Dheerendra P, Joly O, Hunter D, Balezeau F, Sun L, Rees A, Petkov CI, Thiele A, Griffiths TD, 2017. Auditory motion-specific mechanisms in the primate brain. PLOS Biol. 15, e2001379. doi:10.1371/journal.pbio.2001379. [PubMed: 28472038]

Power JD, Barnes KA, Snyder AZ, Schlaggar BL, Petersen SE, 2012. Spurious but systematic correlations in functional connectivity MRI networks arise from subject motion. Neuroimage 59, 2142–2154. doi:10.1016/j.neuroimage.2011.10.018. [PubMed: 22019881]

Premereur E, Van Dromme IC, Romero MC, Vanduffel W, Janssen P, 2015. Effective connectivity of depth-structure–selective patches in the lateral bank of the macaque intraparietal sulcus. PLOS Biol. 13, e1002072. doi:10.1371/journal.pbio.1002072. [PubMed: 25689048]

Randerath J, Goldenberg G, Spijkers W, Li Y, Hermsdörfer J, 2010. Different left brain regions are essential for grasping a tool compared with its subsequent use. Neuroimage 53, 171–180. doi:10.1016/j.neuroimage.2010.06.038. [PubMed: 20600986]

Rinne T, Muers RS, Salo E, Slater H, Petkov CI, 2017. Functional imaging of audio–visual selective attention in Monkeys and humans: how do lapses in Monkey performance affect cross-species correspondences? Cereb. Cortex 27, 3471–3484. doi:10.1093/cercor/bhx092. [PubMed: 28419201]

Salimi-Khorshidi G, Douaud G, Beckmann CF, Glasser MF, Griffanti L, Smith SM, 2014. Automatic denoising of functional MRI data: combining independent component analysis and hierarchical fusion of classifiers. Neuroimage 90, 449–468. doi:10.1016/j.neuroimage.2013.11.046. [PubMed: 24389422]

Schönwiesner M, Dechent P, Voit D, Petkov CI, Krumbholz K, 2015. Parcellation of human and Monkey core auditory cortex with fMRI pattern classification and objective detection of

tonotopic gradient reversals. Cereb. Cortex 25, 3278–3289. doi:10.1093/cercor/bhu124. [PubMed: 24904067]

Schwiedrzik CM, Zarco W, Everling S, Freiwald WA, 2015. Face patch resting state networks link face processing to social cognition. PLOS Biol. 13, e1002245. doi:10.1371/journal.pbio.1002245. [PubMed: 26348613]

Shumaker RW, Walkup KR, Beck BB, 2011. Animal Tool Behavior: The Use and Manufacture of Tools by Animals. JHU Press.

Slater H, Milne AE, Wilson B, Muers RS, Balezeau F, Hunter D, Thiele A, Griffiths TD, Petkov CI, 2016. Individually customisable non-invasive head immobilisation system for non-human primates with an option for voluntary engagement. J. Neurosci. Methods 269, 46–60. doi:10.1016/j.jneumeth.2016.05.009. [PubMed: 27189889]

Smith SM, Beckmann CF, Andersson J, Auerbach EJ, Bijsterbosch J, Douaud G, Duff E, Feinberg DA, Griffanti L, Harms MP, Kelly M, Laumann T, Miller KL, Moeller S, Petersen S, Power J, Salimi-Khorshidi G, Snyder AZ, Vu AT, Woolrich MW, Xu J, Yacoub E, Uğurbil K, Van Essen DC, Glasser MF, 2013. Resting-state fMRI in the human connectome project. Neuroimage 80, 144–168. doi:10.1016/j.neuroimage.2013.05.039. [PubMed: 23702415]

Stevens WD, Tessler MH, Peng CS, Martin A, 2015. Functional connectivity constrains the category-related organization of human ventral occipitotemporal cortex: Connectivity constrains VOTC organization. Hum. Brain Mapp 36, 2187–2206. doi:10.1002/hbm.22764. [PubMed: 25704493]

Tarhan LY, Watson CE, Buxbaum LJ, 2015. Shared and distinct neuroanatomic regions critical for tool-related action production and recognition: evidence from 131 left-hemisphere stroke patients. J. Cogn. Neurosci 27, 2491–2511. doi:10.1162/jocn_a_00876. [PubMed: 26351989]

Touwen BCL, 1995. The neurological development of prehension: a developmental neurologist's view. Int. J. Psychophysiol 19, 115–127. doi:10.1016/0167-8760(94)00080-X. [PubMed: 7622408]

Tsao DY, Moeller S, Freiwald WA, 2008. Comparing face patch systems in macaques and humans. Proc. Natl. Acad. Sci 105, 19514–19519. doi:10.1073/pnas.0809662105. [PubMed: 19033466]

Vaesen K, 2012. The cognitive bases of human tool use. Behav. Brain Sci 35, 203–218. doi:10.1017/S0140525X11001452. [PubMed: 22697258]

Van Essen DC, Donahue CJ, Coalson TS, Kennedy H, Hayashi T, Glasser MF, 2019. Cerebral cortical folding, parcellation, and connectivity in humans, nonhuman primates, and mice. Proc. Natl. Acad. Sci 116, 26173–26180. doi:10.1073/pnas.1902299116.

Van Essen DC, Smith SM, Barch DM, Behrens TEJ, Yacoub E, Ugurbil K, 2013. The WU-Minn human connectome project: an overview. Neuroimage 80, 62–79. doi:10.1016/j.neuroimage.2013.05.041. [PubMed: 23684880]

Visalberghi E, Limongelli L, 1994. Lack of comprehension of cause-effect relations in tool-using capuchin Monkeys (Cebus apella). J. Comp. Psychol 108, 15–22. [PubMed: 8174341]

Wang X, Zhen Z, Song Y, Huang L, Kong X, Liu J, 2016. The hierarchical structure of the face network revealed by its functional connectivity pattern. J. Neurosci 36, 890–900. doi:10.1523/JNEUROSCI.2789-15.2016. [PubMed: 26791218]

Wang X, Zhuang T, Shen J, Bi Y, 2018. Disentangling representations of shape and action components in the tool network. Neuropsychologia 117, 199–210. doi:10.1016/j.neuropsychologia.2018.05.026. [PubMed: 29859296]

Wang Y, Metoki A, Smith DV, Medaglia JD, Zang Y, Benear S, Popal H, Lin Y, Olson IR, 2020. Multimodal mapping of the face connectome. Nat. Hum. Behav 4, 397–411. doi:10.1038/s41562-019-0811-3. [PubMed: 31988441]

Watson CE, Buxbaum LJ, 2015. A distributed network critical for selecting among tool-directed actions. Cortex 65, 65–82. doi:10.1016/j.cortex.2015.01.007. [PubMed: 25681649]

Wilson B, Kikuchi Y, Sun L, Hunter D, Dick F, Smith K, Thiele A, Griffiths TD, Marslen-Wilson WD, Petkov CI, 2015. Auditory sequence processing reveals evolutionarily conserved regions of frontal cortex in macaques and humans. Nat. Commun 6, 8901. doi:10.1038/ncomms9901. [PubMed: 26573340]

Wu J, Ngo GH, Greve D, Li J, He T, Fischl B, Eickhoff SB, Yeo BTT, 2018. Accurate nonlinear mapping between MNI volumetric and FreeSurfer surface coordinate systems. Hum. Brain Mapp 39, 3793–3808. doi:10.1002/hbm.24213. [PubMed: 29770530]

Wu W, Wang X, Wei T, He C, Bi Y, 2020. Object parsing in the left lateral occipitotemporal cortex: whole shape, part shape, and graspability. Neuropsychologia 138, 107340. doi:10.1016/j.neuropsychologia.2020.107340. [PubMed: 31935393]

Xia M, Wang J, He Y, 2013. BrainNet viewer: a network visualization tool for human brain connectomics. PLoS One 8, e68910. doi:10.1371/journal.pone.0068910. [PubMed: 23861951]

Xu T, Nenning KH, Schwartz E, Hong SJ, Vogelstein JT, Goulas A, Fair DA, Schroeder CE, Margulies DS, Smallwood J, Milham MP, Langs G, 2020. Cross-species functional alignment reveals evolutionary hierarchy within the connectome. Neuroimage 223, 117346. doi:10.1016/j.neuroimage.2020.117346. [PubMed: 32916286]

Yan CG, Wang XD, Zuo XN, Zang YF, 2016. DPABI: data processing & analysis for (resting-state) brain imaging. Neuroinformatics 14, 339–351. doi:10.1007/s12021-016-9299-4. [PubMed: 27075850]

Yarkoni T, Poldrack RA, Nichols TE, Van Essen DC, Wager TD, 2011. Large-scale automated synthesis of human functional neuroimaging data. Nat. Methods 8, 665–670. doi:10.1038/nmeth.1635. [PubMed: 21706013]

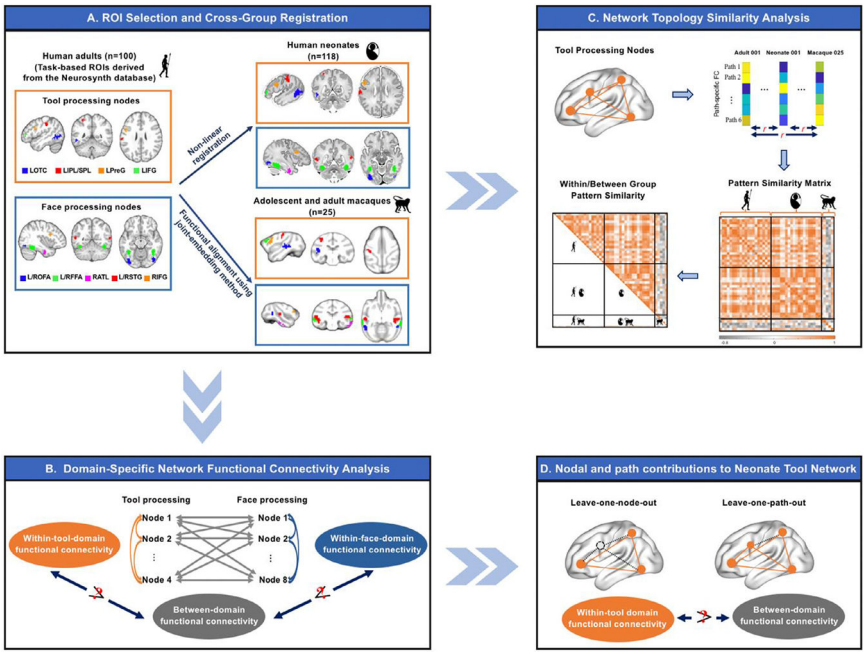

Fig. 1.

Flow chart of resting-state functional connectivity (rsFC) analyses for tool and face processing networks in human adults, human neonates and macaques. A. Tool and face processing nodes are presented in slice views on standard templates for human adults (T1-weighted), human neonates (T2-weighted), and macaques (T1-weighted). These nodes were initially derived from task-based fMRI meta-analyses using the Neurosynth database and then registered to human neonate and macaque spaces using non-linear registration and functional alignment approaches, respectively. B. Intrinsic networks were first evaluated by comparing rsFC between nodes of the same network to that of nodes belonging to different networks. C. A step-by-step procedure is illustrated for computing network topology similarity between groups (using the tool processing network as an example). D. Additional characterization of nodal and path contributions to the formation of the tool processing network using the leave-one-out approach. Slice views and projected brain images were prepared in Mricron (https://www.nitrc.org/projects/mricron) and BrainNet Viewer (Xia et al., 2013), respectively. LOTC: left lateral occipitotemporal cortex; LIPL/SPL: left inferior and superior parietal lobule; LPreG: left premotor gyrus; LIFG: left inferior frontal gyrus; L/ROFA: left and right occipital face areas; L/RFFA: left and right fusiform face areas; RATL: right anterior temporal lobe; L/RSTG: left and right superior temporal gyrus; RIFG: right inferior frontal gyrus.

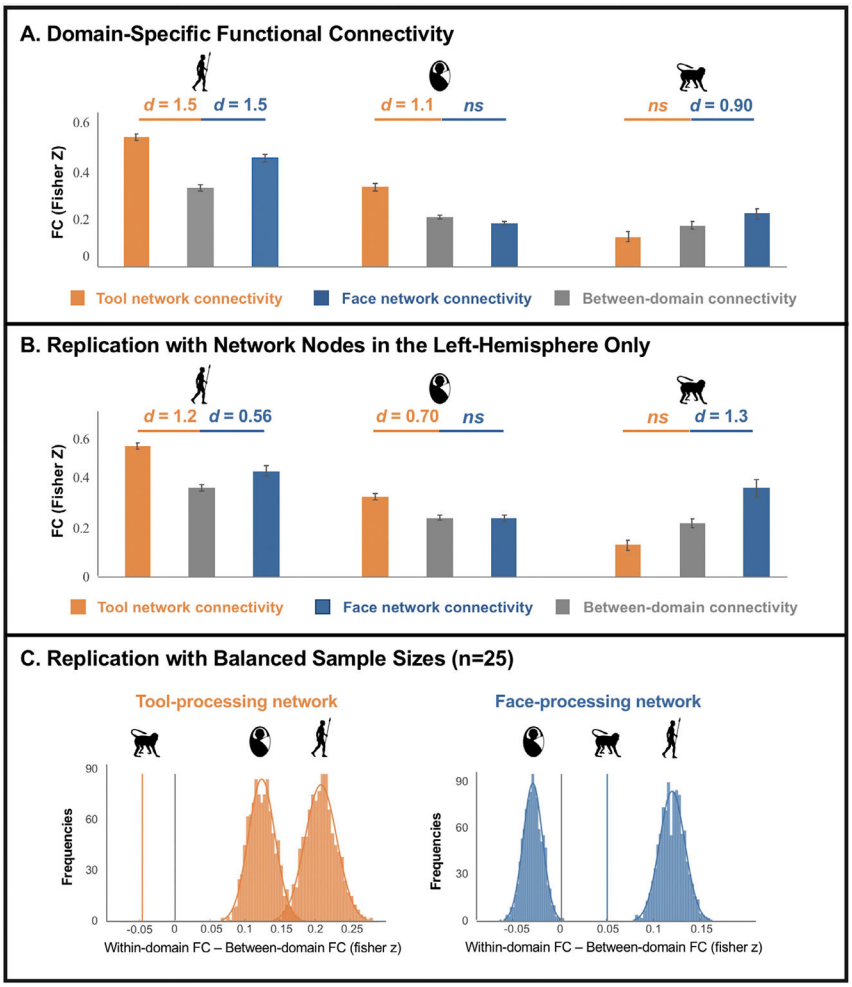

Fig. 2.

The human adult tool-network intrinsic connectivity structure is present in human neonates, but not in adolescent/mature macaques. A. Bar graphs illustrate resting-state functional connectivity (rsFC) values for within-domain and between-domain connectivity in all three groups. Effect sizes (Cohen's d) are shown for comparisons in which significantly greater within-domain than between-domain rsFC was observed (all $p_{corrected} < 0.001$). Error bars indicate standard errors. B. Bar graphs depict replication results for the network analysis using only left-hemispheric nodes. The tool processing nodes lying in the left hemisphere showed shorter path length of the within-tool-domain connections compared to that of the between-domain connections in all three groups (all $p < 0.05$), which might confound with the observed tool network effects. A validation analysis was thus conducted with only ROIs in the left hemisphere to ensure balanced within-tool-domain and between-domain nodal distances (see Supplementary Materials 1.1 for details). Effect sizes (Cohen's d) are shown for comparisons in which significantly greater within-domain than between-domain rsFC was observed (all $p_{corrected} < 0.001$). Error bars indicate standard errors. C. Distribution maps show network effects from the bootstrapping analysis (n=10,000) in human adults and neonates, which were calculated as within-domain minus between-domain rsFC (rsFC differences) for tool and face processing networks based on subgroups of

randomly selected human adults and neonates (n = 25, equal to the sample size of macaques, see Supplementary Materials 1.1 for details). A single line is used to indicate the rsFC differences for macaques, since no bootstrapping analyses were performed in this group. The grey line represents 0.

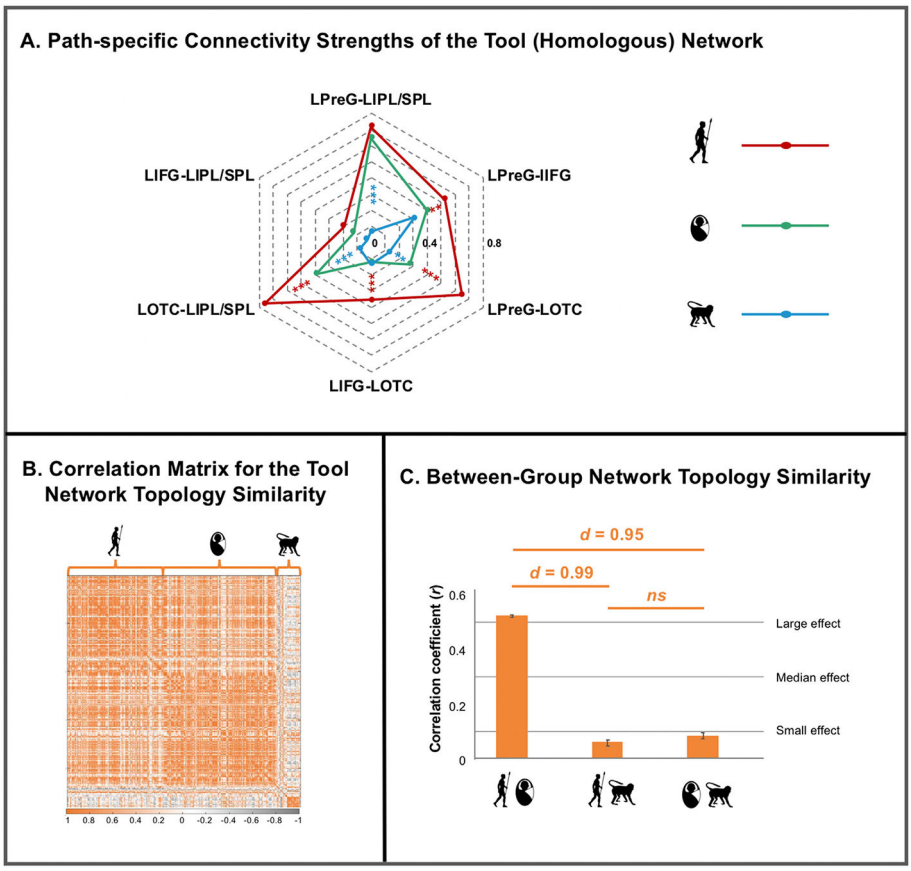

Fig. 3.

High topological similarities for the tool (homologous) network between human adults and neonates, but not between humans and macaques. A. Path-specific connectivity strengths (Fisher Z scores) of the tool (homologous) network in all three groups. Significant group comparisons between human adults and human neonates are marked in *, whereas significant group differences between human neonates and macaques are marked in *. The left premotor-left inferior/superior parietal path was species-specific, since it was the only path that was comparable between human adults and human neonates, but different between human neonates and macaques. * $p_{corrected} < 0.05$, ** $p_{corrected} < 0.01$, *** $p_{corrected} < 0.001$. B. The correlational matrix for the network topology similarities in all three populations for the tool processing network. C. Bar graphs show tool network topology similarities for participants belonging to different groups. Effect sizes (Cohen's d) are shown for comparisons in which significant differences in between-group pattern similarities were observed (all $p_{corrected} < 0.001$). Error bars indicate standard errors.

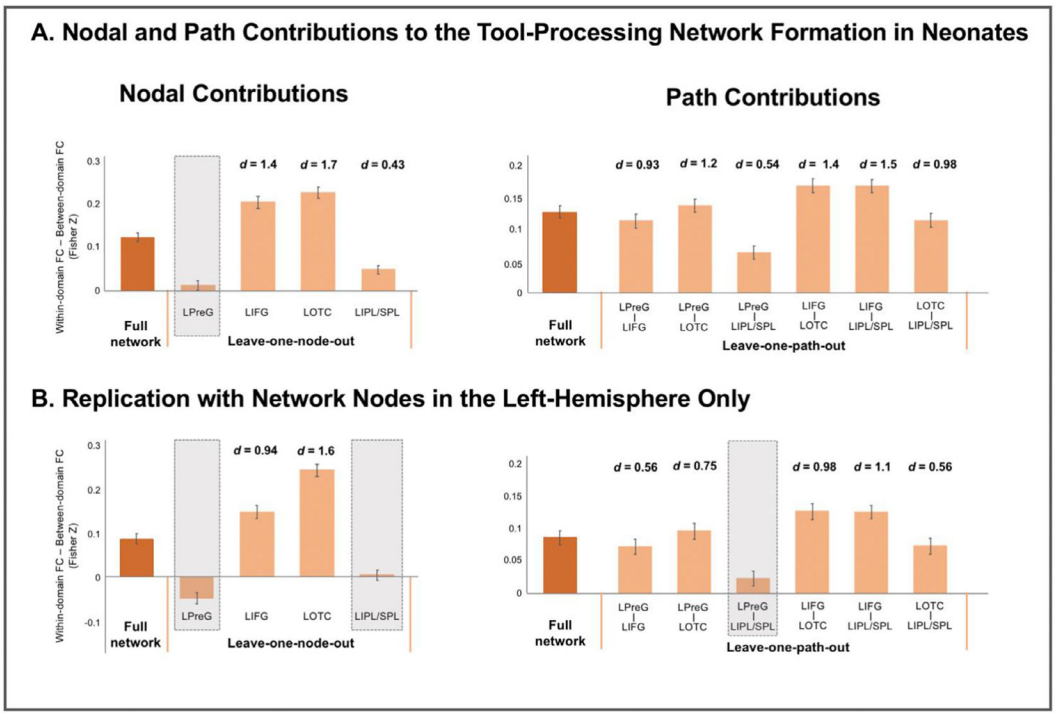

Fig. 4.

Critical contributions of the premotor region and its connectivity with the parietal region to the formation of the intrinsic tool homologous network in human neonates, as revealed by leave-one-node/path-out analyses. A. Bar graphs illustrate network effects, calculated as within-domain minus between-domain rsFC, for the full tool network and when each of the constituent nodes (left column) or path (right column) is removed. B. Bar graphs exhibit results of the leave-one-node/path out analysis derived from left-hemispheric nodes with balanced within-tool-domain and between-domain path length. Effect sizes (Cohen's d) are shown when the rsFC of the remaining tool network were still significantly higher than that of the between-domain connections (all $p_{\text{corrected}} < 0.001$). Error bars indicate corresponding standard errors. LOTC: left lateral occipitotemporal cortex; LIPL/SPL: left inferior and superior parietal lobule; LPreG: left premotor gyrus; LIFG: left inferior frontal gyrus; rsFC: resting-state functional connectivity